Published in final edited form as:
Dev Cell. 2013 February 11; 24(3): 296–309. doi:10.1016/j.devcel.2012.12.003.

Wnt-dependent epithelial transitions drive pharyngeal pouch formation

Chong Pyo Choe[1], **Andres Collazo**[2,3], **Le A. Trinh**[4], **Luyuan Pan**[5], **Cecilia B. Moens**[5], and **J. Gage Crump**[1,3,*]

[1]Broad California Institute of Regenerative Medicine Center, Keck School of Medicine, University of Southern California, Los Angeles, CA 90033, USA

[2]House Research Institute, Los Angeles, CA 90057, USA

[3]Department of Cell and Neurobiology, Keck School of Medicine, University of Southern California, Los Angeles, CA 90033, USA

[4]Biological Imaging Center, California Institute of Technology, Pasadena, CA 91125, USA

[5]Howard Hughes Medical Institute and Division of Basic Science, Fred Hutchinson Cancer Research Center, Seattle, WA 98109, USA

SUMMARY

The pharyngeal pouches, which form by budding of the foregut endoderm, are essential for segmentation of the vertebrate face. To date, the cellular mechanism and segmental nature of such budding have remained elusive. Here, we find that Wnt11r and Wnt4a from the head mesoderm and ectoderm, respectively, play distinct roles in the segmental formation of pouches in zebrafish. Time-lapse microscopy, combined with mutant and tissue-specific transgenic experiments, reveal requirements of Wnt signaling in two phases of endodermal epithelial transitions. Initially, Wnt11r and Rac1 destabilize the endodermal epithelium to promote the lateral movement of pouch-forming cells. Next, Wnt4a and Cdc42 signaling induce the rearrangement of maturing pouch cells into bilayers through junctional localization of the Alcama immunoglobulin-domain protein, which functions to restabilize adherens junctions. We propose that this dynamic control of epithelial morphology by Wnt signaling may be a common theme for the budding of organ anlagen from the endoderm.

INTRODUCTION

As with the vertebral skeleton, the craniofacial skeleton forms from a series of segments, the pharyngeal arches. During embryogenesis, a series of outpocketings, termed pouches, develop in an anterior-posterior wave from the pharyngeal endoderm (PE). These pouches then segment the cranial-neural-crest-derived precursors of the facial skeleton into distinct arches. The pouches also contribute to a number of important organs in the face and neck, including the Eustachian tube, thymus, and parathyroid (Peters et al., 1998), and have important signaling functions in the later development of the skeleton, muscle, nerves and epithelia derived from the arches (Graham et al., 2005). Surprisingly then, given the central

*Correspondence: J. Gage Crump gcrump@usc.edu, Phone: (323) 442-2693, Fax: (323) 442-4040.

role of pouches in organizing the head, little is known about the molecular and cellular mechanisms underlying their segmental development.

The number of pharyngeal pouches is highly variable among vertebrates - ranging from four in mice to as many as sixteen in hagfish – and hence PE segmentation is likely an indeterminate process (Graham, 2008). Zebrafish form six pouches, with the first and second pouches forming simultaneously at 18 hours post-fertilization (hpf) and the third through sixth forming successively from 20-36 hpf (Crump et al., 2004). Previously, we showed that pouches form by the lateral movement of PE cells, with Fgf3 and Fgf8a, in part from the mesoderm, being required for this migration (Crump et al., 2004). The segmentation of the PE into pouches appears not to require neural crest, as pouches form in avians and mice experimentally lacking neural crest and in chordates in which neural crest has not evolved (Graham, 2001). One possibility is that PE segmentation involves a cell-autonomous oscillatory mechanism akin to the “clock-wavefront” model proposed for somitic mesoderm segmentation (Dequeant and Pourquie, 2008). Alternatively, older studies have suggested the presence of segmented ectoderm (ectomeres) and mesoderm (somitomeres) in the head, and hence head endoderm segmentation could result secondarily from ectodermal and/or mesodermal signals (Couly and Le Douarin, 1990; Jacobson, 1988; Meier, 1979). Here, we present evidence that segmental Wnt signals from the mesoderm and ectoderm cooperatively instruct head endoderm segmentation.

A feature of epithelial morphogenesis is that cells undergo dynamic transitions in morphology and neighbor relationships that promote tissue remodeling. Wnt signaling has been implicated in multiple contexts in controlling cell shape and rearrangements that drive tissue morphogenesis, such as during vertebrate axis elongation. This morphogenetic function of Wnt signaling appears to be largely independent from nuclear-β-catenin-mediated transcriptional regulation, instead involving a number of cytoplasmic effectors including the small GTPases Rho, Rac, and Cdc42 (Schlessinger et al., 2009). For example, activation of Rac at the leading edge of cells is sufficient to promote directional migration (Yoo et al., 2010), and Cdc42 is required for the morphology and apicobasal polarity of epithelial cells in the *Drosophila* embryo (Eaton et al., 1995; Hutterer et al., 2004) and vertebrate pancreas (Kesavan et al., 2009). By studying zebrafish mutants and embryos with PE-specific disruption of putative Wnt effectors, we show here that Wnts control distinct steps of pouch epithelial morphogenesis: a Wnt11r-Rac1 pathway that initially destabilizes the epithelium to allow remodeling and a Wnt4a-Cdc42 pathway that restabilizes the epithelium to form mature pouch bilayers.

Epithelial cells maintain tight connections in part through adherens junctions (AJs) composed of cadherin-class cell adhesion molecules (CAMs) and associated proteins such as α-catenin (Friedl and Gilmour, 2009). In order for epithelial remodeling to take place, these AJs presumably must be very dynamic to allow the rearrangement of cells. Previous studies suggest various potential mechanisms of AJ remodeling during epithelial morphogenesis, such as endocytosis and degradation of cadherins (Nishimura and Takeichi, 2009) and the sliding of AJs along the lateral membranes of cells (Wang et al., 2012). How AJs are dynamically controlled within developing vertebrate epithelia remains less understood. Here, we provide evidence for a remarkably specific requirement of Activated Leukocyte Cell Adhesion Molecule (ALCAM; also known as CD166, Neurolin, or DM-GRASP) for the restabilization of AJs during pouch bilayer formation. ALCAM is an immunoglobulin (Ig)-CAM that has been reported to have diverse roles in neuronal cell migration, neurite extension, cardiac morphogenesis, B-lymphoma development, and neural crest differentiation (Abo et al., 1991; Choudhry et al., 2011; Gessert et al., 2008; Lawrence et al., 2002; Lee et al., 1996; Tomita et al., 2000), yet its role in epithelial transitions had not previously been investigated. We find zebrafish *alcama* to be prominently expressed in

developing pouches, with Alcama protein localizing to cell-cell junctions in a Wnt4a/Cdc42-dependent manner. Moreover, we find that depletion of Alcama from embryos results in a failure of maturing pouches to stabilize AJs and transition from a multilayered to a bilayered morphology. Hence, our studies reveal a specific regulatory role of this Ig-CAM in re-establishing highly organized epithelia after initial remodeling.

RESULTS

Pouch formation involves dynamic epithelial transitions in association with *nkx2.5*-expressing mesoderm

In order to observe epithelial cell behaviors during in vivo pouch formation, we constructed a zebrafish transgenic line (*her5*:mCherryCAAX) in which a membrane-tethered mCherry fluorescent protein was expressed under the endodermal *her5* promoter (Tallafuss and Bally-Cuif, 2003). As we had previously shown that the adjacent mesoderm is a source of Fgfs for pouch formation (Crump et al., 2004), we also used a *nkx2.5*:GFP transgenic line (Witzel et al., 2012) to simultaneously visualize mesoderm dynamics. Time-lapse recordings of doubly transgenic embryos from 18-34 hpf showed that the initiation of *nkx2.5*:GFP expression in mesoderm coincided with the A-P formation of pouches (Movie S1). Higher magnification recordings further revealed dynamic transitions in pouch epithelial morphology (3-D projection in Figure 1A-E; representative section in Figure 1F-J; and Movie S2). Prior to pouch formation (e.g. pouch (p) 5 in Figure 1B,G), the PE consists of a bilayer sheet across the midline. The first indication of pouch initiation is that a subset of cells within the PE bilayer adopt a less elongated morphology and become multilayered, with faint *nkx2.5*:GFP expression becoming apparent in adjacent mesoderm (e.g. p5 in Figure 1C,H). In this transitional epithelium, multilayered cells now collectively translocate to more dorsal-lateral positions while maintaining close association and/or direct contacts with *nkx2.5*:GFP-expressing mesoderm (e.g. p5 in Figure 1D,I and p4 in Figure 1A,F). Finally, cell tracking shows that pouch cells rearrange into mature bilayers along the dorsal-lateral axis (e.g. p5 in Figure 1E,J and p4 in Figure 1C,H). Together, our observations indicate two important epithelial transitions during wild-type pouch formation: an initial transition from a bilayered to a multilayered morphology that coincides with collective cell migration, and a later transition that reestablishes the bilayer as pouches mature.

As we observed intimate interactions of PE and mesoderm throughout pouch morphogenesis, we also investigated the requirement for *nkx2.5*:GFP+ mesoderm by transgenic ablation in *nkx2.5*:Gal4VP16; UAS:CFP-NTR embryos. Nitroreductase (NTR) mediates the conversion of metronidazole (Mtz) into a toxic substance in a cell-autonomous manner (Curado et al., 2008). Whereas untreated *nkx2.5*:Gal4VP16; UAS:CFP-NTR embryos displayed specific CFP fluorescence in the head mesoderm (Figure 1K), one-cell-stage injection of Mtz resulted in major reductions of CFP-positive mesoderm by 35 hpf (Figure 1M). Consistent with a role for *nkx2.5*-expressing mesoderm in pouch formation, Mtz-mediated ablation of head mesoderm resulted in malformations of the posterior pouches compared to un-injected siblings (Figure 1L,N).

wnt11r, wnt4a, and *fzd8a* are expressed in pouch-forming regions

As Wnt signaling has well known roles in epithelial cell behavior, we next investigated the expression of specific Wnt ligands and receptors during pouch formation. In particular, *wnt11r* expression was first seen in a single spot near the developing third pouch at 24 hpf, with expression spreading to additional foci adjacent to more posterior pouches by 28 hpf (Figure 2A,B). *wnt4a* was also segmentally expressed adjacent to developing pouches (Figure 2C,D). However, co-localization with *nkx2.5* revealed that *wnt11r* was expressed in the mesoderm yet *wnt4a* was expressed in the overlying ectoderm (Figure 2G-J). Somewhat

unexpectedly, both *wnt11r* and *wnt4a* expression were reduced upon Mtz-mediated ablation of head mesoderm, suggesting a non-autonomous role of the mesoderm in ectodermal *wnt4a* expression (Figure 2M-P). In a complementary manner, we found *fzd8a*, a member of the Frizzled (Fzd) class of G-protein-coupled receptors that transduce Wnt signaling in a variety of contexts (Wodarz and Nusse, 1998), to be expressed in the *her5*:GFP-positive pouch-forming endoderm (Figure 2E,F,K), consistent with previous reports of *fzd8a* expression in pouch endoderm at later stages (55 hpf) (Sisson and Topczewski, 2009).

Distinct requirements of Wnt11r and Wnt4a in pouch formation

In order to determine requirements for Wnt11r and Wnt4a in pouch formation, we next examined $wnt11r^{fh224}$ (Banerjee et al., 2011) and $wnt4a^{fh295}$ alleles, which result in nonsense mutations after amino acids 31 and 341, respectively. Indeed, both *wnt11r* and *wnt4a* single mutants had partially penetrant defects in posterior pouch formation, with more severe defects observed in double mutants (Figure 3B-D and Table 1). Although the $wnt4a^{fh295}$ mutation truncates only a small C-terminal fragment of the protein, phenocopy with a *wnt4a* morpholino (MO) confirmed it as a loss-of-function allele (Figure S1B,M and Table 1). In order to confirm that pouch development was not simply delayed in mutants, we also examined development of the five ceratobranchial cartilages (CBs) at 5 days-post-fertilization (dpf), whose segmentation and differentiation are pouch-dependent (Piotrowski and Nusslein-Volhard, 2000). Consistent with the observed pouch defects, single and double mutants displayed fusions and reduced numbers of CBs (Figure 3N-P and Table 1) despite arch neural crest specification (*sox10* expression at 14 hpf), arch formation (*dlx2a* at 16.5 hpf), and later dorsoventral patterning (*dlx2a* and *dlx3b* at 32 hpf) being unaffected in mutants (as well as Wnt misexpression embryos – see below) (Figure S1N-P).

Whereas both *wnt11r* and *wnt4a* mutants displayed pouch and CB defects, a closer examination revealed differences in the nature of pouch defects. In *wnt11r* mutants, there were a reduced number of pouches and the most posterior pouches appeared to be delayed in their outgrowth (Figure 4J and Table 1). In contrast, *wnt4a* mutants had normal numbers of pouches, yet cells within these pouches were inappropriately multilayered (Figure 4K and Table 1). In order to understand the cellular basis of these different phenotypes, we next made time-lapse movies of pouch development in these mutants. In particular, we focused on development of the fifth pouch, as it was the pouch most consistently affected in mutants. Strikingly, tracking of *her5*:mCherryCAAX+ cells revealed opposite defects in pouch cell behavior. Whereas the migration of $wnt11r^{-/-}$ pre-pouch cells was delayed compared to wild-type cells, $wnt4a^{-/-}$ pouch-forming cells migrated faster yet failed to resolve into bilayers (n=3 for each genotype) (Figure 3Y-AB and Movie S3). These findings are consistent with an early role of Wnt11r in initiating pouch outgrowth and a later role of Wnt4a in terminating pouch outgrowth as cells organize into bilayers.

Ectopic Wnt11r or Wnt4a has distinct effects on pouch morphogenesis

The distinct requirements of Wnt11r and Wnt4a in pouch cell behaviors could reflect differences in their patterns of expression, or alternatively differential activation of downstream signaling cascades. In order to distinguish between these possibilities, we tested whether misexpression of these ligands in the forming endoderm also resulted in distinct effects on pouch cell behavior. To do so, we developed an *nkx2.3*:Gal4VP16 line which drives UAS transgene expression specifically in the PE from 18 hpf onwards (Figure S2A), consistent with endogenous *nkx2.3* expression (Lee et al., 1996). Combining this *nkx2.3*:Gal4VP16 line with UAS:Wnt11r and UAS:Wnt4a transgenes thus allowed us to widely misexpress these Wnts during pouch formation. Consistent with localized expression of these ligands being important for pouch formation, misexpression of either Wnt11r or Wnt4a disrupted pouch and CB cartilage development (Figure 3E,F,Q,R). Interestingly,

Wnt4a misexpression resulted in the formation of bilayer-like structures in inappropriate domains of PE, yet Wnt11r misexpression caused a fragmentation of the epithelium into small rosettes that was indicative of a loss of epithelial integrity (Figure 4N,O). These results suggest that the distinct requirements of Wnt11r and Wnt4a in pouch cell behaviors are not simply due to their specific expression domains. Instead, these Wnts appear to have distinct signaling functions, with Wnt11r destabilizing the epithelium and Wnt4a promoting bilayer formation.

A requirement of Fzd8a for Wnt11r and Wnt4a signaling in pouches

As we observed Fzd8a, a putative Wnt receptor, to be expressed in forming pouches, we next analyzed its requirement in pouch development. Consistent with a role of Fzd8a in mediating both Wnt11r and Wnt4a signaling, depletion of Fzd8a with either a previously validated MO (Kim et al., 2002) or a second translation-blocking MO resulted in similar losses and fusions of pouches and CBs as seen in *wnt11r; wnt4a* double mutants (Figure 3G,S; Figure S1C,I; and Table 1). *fzd8a*-MO defects were not further enhanced by loss of *wnt11r* or *wnt4a*, as expected if Fzd8a acts downstream of these Wnts, although we did detect a modest enhancement in the *wnt4a*$^{-}$*; wnt11r*$^{-}$*; fzd8a*-MO triple combination (Figure S1D,J and Table 1). Also implicating Wnt4a, Wnt11r, and Fzd8a in a common genetic pathway, a sub-threshold dose of *fzd8a*-MO enhanced *wnt4a*$^{-}$ and *wnt11r*$^{-}$ single mutant defects (Table 1). Moreover, depletion of Fzd8a suppressed the distinct changes in epithelial morphology seen upon Wnt11r and Wnt4a misexpression (Figure 4P,Q). Together, our loss-of-function and epistasis data support a role for Fzd8a in mediating both Wnt11r and Wnt4a activity in developing pouches.

Dvl and Rac signaling promote pouch initiation

Wnt11r and Wnt4a have been implicated in nuclear-β-catenin-independent signaling in other contexts (Matsui et al., 2005). In order to determine whether pouch formation also relies on nuclear-β-catenin-independent signaling, we used our *nkx2.3*:Gal4VP16 driver to express either a dominant-negative (DN) form of Tcf7l2 (DN-Tcf7l2) that inhibits ß-catenin-dependent transcription (Molenaar et al., 1996; van de Wetering et al., 2002) or a DN form of Dvl that lacks the DEP domain (DvlΔDEP) and inhibits cytoplasmic Dvl signaling but not ß-catenin-dependent transcription (Axelrod et al., 1998). Consistent with pouch formation being nuclear-β-catenin-independent, PE-specific misexpression of DvlΔDEP resulted in severe pouch and CB defects (Figure 3H,T and Table 1), yet PE-specific expression of DN-Tcf7l2 caused no such defects (Figure S1A,G), despite it causing defects when expressed in the mesoderm (data not shown). In addition, time-lapse recordings of *nkx2.3*:Gal4VP16; UAS:DvlΔDEP; *her5*:mCherryCAAX embryos from 24-32 hpf (n=3) revealed that the loss of pouches was due to a failure of PE cells to become multilayered and collectively migrate dorsal-laterally (Movie S4). Further consistent with a role of Dvl in pouch formation, we also observed transient localization of GFP-Dvl to apical membranes of pouch-forming cells in time-lapse recordings of *nkx2.3*:GFP-Dvl; *her5*:mCherryCAAX embryos (n=3) (Figure S2B and Movie S5). Such apical localization of Dvl has been shown to correlate with its activation in other epithelial cell types (Park et al., 2008).

As small GTPases are common effectors of Wnt and Dvl signaling during cell migration and epithelial morphogenesis (Schlessinger et al., 2009), we next investigated the role of the small GTPase Rac in pouch formation. To do so, we used the *nkx2.3*:Gal4VP16 driver to express T17N DN (Feig, 1999) and G12V constitutively active (CA) (Abo et al., 1991) versions of Rac1 in the pre-pouch endoderm. Consistent with a requirement of Rac in pouch formation, misexpression of DN-Rac1 resulted in reductions and fusions of pouches and CBs (Figure 3I,U and Table 1). In confirmation of our DN results, pharmacological inhibition of Rac with NSC23766 from 18-26 hpf resulted in similar but more severe pouch

and CB defects (Figure S1F,L). Although PE-specific misexpression of CA-Rac1 also caused severe defects in pouch and CB development (Figure 3J,V and Table 1), a closer analysis revealed dramatically different effects of DN-Rac1 and CA-Rac1 on pouch morphology. Whereas Rac inhibition resulted in a variable loss of pouch extension (Figure S3C), constitutive Rac activation caused the PE to fragment into small rosette-like structures (Figure 4S). These differences were particular apparent in time-lapse recordings. Whereas DN-Rac1 PE cells had a delay in collective migration (n=5, Movie S4), nearly all epithelial cells in the CA-Rac1 pre-pouch endoderm were multilayered and highly motile, and eventually fragmented into rosette-like structures (n=3, Movie S4). Intriguingly, both Wnt11r and CA-Rac1 misexpression induced similar rosette-like morphologies, suggesting that Rac1 might act downstream of Wnt11r-Fzd8a signaling for the initial destabilization of the pre-pouch endoderm. Consistently, CA-Rac1 was able to generate rosette-like PE structures in the absence of Wnt11r (Figure 4T) or Fzd8a (Figure S3A).

Cdc42 controls pouch epithelial morphology through junctional localization of Alcama

In the course of our analysis using the anti-Alcama antibody to label pouches, we noticed that reduced Wnt4a, Fzd8a, or Dvl function had dramatic effects on membrane localization of the Alcama Ig-CAM protein. During wild-type pouch development, *alcama* expression begins as PE cells remodel, at which time Alcama protein is weakly and diffusely localized within cells (Figure 4A). As pouch development proceeds, Alcama becomes progressively enriched at sites of cell-cell contact along apical and lateral plasma membranes (Figure 4B-D). Time-lapse recordings of pouch development in *nkx2.3*:Alcama-GFP; *her5*:mCherryCAAX transgenic embryos, in which a functional Alcama-GFP fusion protein (see below) was expressed specifically in PE cells, confirmed the progressive localization of Alcama to cell-cell contacts during pouch development (n=3) (Figure 4E-H and Movie S6). The progressive membrane localization of Alcama-GFP indicates that membrane accumulation is not simply due to increased expression of the *alcama* gene, as the fusion protein was expressed from a heterologous promoter. Consistent with a role of Wnt4a, Fzd8a and Dvl in asymmetric Alcama localization, Alcama was mislocalized from the plasma membrane to the cytoplasm (presumably in vesicular compartments) in *wnt4a*$^{-}$, *wnt4a*-MO, *fzd8a*-MO, and *nkx2.3*:Gal4VP16; *UAS*:DvlΔDEP embryos (Figure 4K,M,R and Figure S1B). In contrast, Alcama localization was unaffected in *wnt11r* mutants and not obviously more defective in compound *wnt11r; wnt4a* versus *wnt4a* single mutants, suggesting a distinct role of Wnt4a in Alcama trafficking that correlates with its requirement in bilayer formation (Figure 4J-L and Table 1).

As the small GTPase Cdc42 has been implicated in epithelial cell morphology/polarity in other contexts (Eaton et al., 1995), we next investigated whether it might function downstream of Wnt4a in mediating polarized Alcama localization. Strikingly, PE-specific misexpression of a T17N DN form of Cdc42 disrupted membrane localization of Alcama, whereas misexpression of a G12V CA form resulted in increased enrichment of Alcama at membranes and a dramatically elongated PE cell shape (Figure 4U,V and Figure S3F). These changes in Alcama localization and pouch cell morphology in Cdc42 loss- and gain-of-function embryos correlated with losses and fusions of pouches and CBs (Figure 3K,L,W,X). Although Alcama was also mislocalized in DN-Rac1 embryos, it localized normally in embryos treated with the Rac inhibitor NSC23766 (Figure S3C-E). As DN versions of GTPases often have promiscuous effects on other members (Feig, 1999), it is possible that DN-Rac1 effects on Alcama localization are due to partial inhibition of Cdc42. However, unlike constitutive activation of Rac1, time-lapse recordings revealed that activation of Cdc42 did not result in whole-scale stimulation of PE motility (n=7) (Movie S4).

While small GTPases are known targets of many pathways, epistasis experiments support Cdc42 being downstream of Wnt4a-Fzd8a signaling in maturing pouches. Wnt4a misexpression resulted in increased Alcama localization in inappropriate regions of the pre-pouch endoderm, and this inappropriate Alcama localization was completely suppressed by DN-Cdc42 misexpression (Figure 4O,W). Reciprocally, CA-Cdc42 rescued the Alcama localization defects and induced a hyper-elongated cell morphology in embryos depleted for Wnt4a or Fzd8a (Figure 4X and Figure S3B). Interestingly, we find this role of Wnt4a-Fzd8a-Dvl-Cdc42 signaling in polarized membrane trafficking to be relatively specific for Alcama. In contrast to Alcama, E-cadherin localizes to cell-cell contacts of PE cells throughout morphogenesis, with E-cadherin becoming increasingly enriched at apico-lateral membranes as pouches mature into bilayers (Figures 4Y-AA and 5G). However, PE-specific inhibition of Dvl did not disrupt E-cadherin membrane localization per se, although it did reduce the later junctional enrichment of E-cadherin seen in wild-type mature pouches (Figure 4AB). Together, our combined data indicate a preferential role for Wnt4a-Fzd8a-Dvl-Cdc42 signaling in Alcama trafficking and pouch cell morphology.

Alcama promotes pouch bilayers by stabilizing α-catenin-containing AJs

As we found Alcama to be a target of Wnt4a and Cdc42 signaling, we next investigated the function of Alcama in pouch morphogenesis. To do so, we injected *her5*:mCherryCAAX embryos with a translation-blocking *alcama*-MO (Diekmann and Stuermer, 2009), which we confirmed effectively depletes Alcama protein levels (Figure 5D). Consistent with a selective role of Alcama in the maturation of pouches into bilayers, *alcama*-MO embryos had a normal complement of pouches that displayed an aberrant multilayered morphology (Figure 5C). These defects were due to a loss of Alcama in pouches as PE-specific restoration of Alcama in *nkx2.3*:Alcama-GFP transgenic embryos partially restored bilayered morphology (Figure S4A,B). As this multilayered pouch phenotype was similar to what we observed upon Cdc42 inhibition, we next asked whether Alcama was the primary downstream target of Cdc42 for pouch morphology. Indeed, Alcama depletion completely suppressed the elongated pouch cell morphology resulting from CA-Cdc42 misexpression (Figure 5E,F and Figure S3F). We therefore conclude that Alcama is a major target of Cdc42 in mediating cell morphology changes that promote mature pouch bilayers.

As AJ dynamics are associated with epithelial remodeling, we next asked whether Alcama might promote pouch cell rearrangements by modulating AJs. As with Dvl inhibition, Alcama depletion did not affect the junctional localization of E-cadherin per se but did prevent its later apical enrichment during pouch maturation (Figure 5G,H). In order to better understand AJ dynamics, we utilized a *Gt(ctnna-citrine)*^{ct3a} transgenic line in which the citrine fluorescent protein has been inserted in-frame to create a functional α-catenin fusion protein. α-catenin is prominently associated with AJs in epithelia, and we observed dynamic changes in α-catenin-citrine localization in developing pouches. Still images (Figure 5I-K) and time-lapse recordings (Figure S4C-E and Movie S7, n=3) revealed that α-catenin-citrine was enriched at apical membranes in the pre-pouch endoderm, became less organized in the transitional, multi-layered epithelium, and then was strongly enriched again at apical membranes of mature pouch bilayers. Strikingly, the expression and polarized membrane trafficking of Alcama correlated with the apical enrichment of α-catenin-citrine in maturing pouches, and Alcama depletion disrupted this apical enrichment (Figure 5L-N and Figure S4F). In order to quantitate α-catenin/AJ dynamics, we next performed fluorescence correlation spectroscopy (FCS). In FCS, the detection of fluorescence fluctuations within a small confocal volume (~0.5 fl) provides quantitative information on diffusion coefficients of fluorescent molecules (Ries et al., 2009). In wild-type embryos, FCS measurements revealed a significant increase in α-catenin mobility from pre-pouch to transitional epithelia that then decreased again in mature epithelia, consistent with dynamic AJ remodeling

underlying pouch formation (Figure 5O). In contrast, FCS measurements in *alcama*-MO embryos revealed a normal initial increase in α-catenin mobility but no subsequent decrease, suggesting a specific regulatory function of Alcama in stabilizing AJs as pouch epithelia mature.

DISCUSSION

Our study reveals distinct requirements of Wnt11r in the initiation of pouches at discrete positions and Wnt4a in the subsequent rearrangement of pouch precursors into epithelial bilayers (Figure 6B). We also provide evidence that Wnt11r and Wnt4a coordinate these two phases of epithelial transitions through distinct small GTPases. Whereas Rac promotes the initial destabilization of the PE into a multilayered transitional epithelium, Cdc42 helps stabilize AJs in maturing pouch bilayers through polarized trafficking of the Ig-CAM Alcama.

Roles for mesoderm and ectoderm in segmentation of the head endoderm

All vertebrate embryos have a segmented structure in the head - the pharyngeal arches – whose development depends on the earlier segmentation of the PE into pouches (Graham et al., 2005). Rather than segmentation being an autonomous property of the endoderm, our studies reveal critical roles of the head mesoderm and ectoderm in pouch segmentation. We had previously shown that the mesoderm was an important source of Fgfs for pouch formation (Crump et al., 2004), and here we show that specific ablation of the *nkx2.5*-positive mesoderm disrupts pouch formation. The segmental expression of *wnt11r* in head mesoderm is also consistent with observations of morphological mesoderm segments – somitomeres – in the head (Meier, 1979) and indicates that the early head mesoderm is segmented at the molecular level. Pouch formation also requires segmental expression of *wnt4a* in the head ectoderm, which suggests combined roles of mesoderm and ectoderm in head endoderm segmentation. Whereas our findings place head mesoderm segmentation upstream of pouch segmentation, how the head mesoderm itself is segmented remains a mystery.

Mesodermal signals may also be more generally required for the budding of organ anlagen from the endoderm. In zebrafish, *wnt2bb* is expressed in the mesoderm directly adjacent to the liver-forming endoderm, and in *prometheus/wnt2bb* mutants the initial outgrowth of the liver bud is delayed (Ober et al., 2006). Interestingly, the sea anemone *Nematostella vectensis*, a basal metazoan animal, has twelve Wnt genes that are expressed in overlapping domains along the primary axis of the planula larva (Kusserow et al., 2005). Although it is less clear whether Wnt expression constitutes a similar code along the vertebrate anterior-posterior axis, an intriguing possibility is that different Wnts from the mesoderm - analogous to the roles of Wnt11r in pouch and Wnt2bb in liver formation - might induce budding of the initial anlagen of many or all endodermal organs (Figure 6A).

Distinct roles of Wnt11r and Wnt4a in two phases of pouch epithelial transitions

The development of endodermal organs, such as the pouch-derived glands, liver, lung, and pancreas, follows a common basic pattern (Hogan and Kolodziej, 2002; O'Rahilly, 1978). Interactions with the adjacent mesenchyme induce the formation of a bud from the endodermal epithelium, which then undergoes progressive branching to form the parenchyma. Here, we find that Wnt signals, in part from the mesoderm-derived mesenchyme, are critical for both the initial remodeling and subsequent rearrangements of epithelial cells into pouch bilayers. Previous MO-based studies had implicated Wnt4a and Wnt11r, as well as Wnt11, in the earlier migration of PE precursors to the midline (Matsui et al., 2005). However, our findings that misexpression of Wnts and conditional inhibition of

Dvl signaling in the later *nkx2.3*-expressing endoderm disrupt pouch development indicate that Wnt signaling has roles in pouch formation independent from earlier PE midline migration. Intriguingly, both loss- and gain-of-function experiments indicate that Wnt11r and Wnt4a have discrete roles in the initial destabilization and subsequent restabilization of the developing pouch epithelium, respectively. Pouch initiation is delayed in *wnt11r* mutants, and ectopic Wnt11r reciprocally causes fragmentation of the PE epithelium into rosette-like structures. This suggests a role of Wnt11r in the initial destabilization events that promote the lateral migration of pre-pouch cells. In contrast, pouch-forming cells displayed increased motility in *wnt4a* mutants yet failed to resolve into bilayers. Alcama was also mislocalized in *wnt4a* but not *wnt11r* mutants, with Wnt4a misexpression resulting in enriched junctional Alcama in inappropriate regions. Hence, Wnt4a has a preferential role in the later Alcama-dependent transition of pouch cells into mature bilayers. Such distinct roles of mesodermal Wnt11r and ectodermal Wnt4a would make sense topographically. Endodermal cells are in contact with the *nkx2.5/wnt11r*-expressing mesoderm at the time of pouch initiation but only contact the *wnt4a*-expressing ectoderm after lateral migration. Although Wnt ligands are known to elicit different types of signaling cascades in recipient cells, how Wnt11r and Wnt4a might mediate distinct pouch cell behaviors remains unclear. Depletion of Fzd8a results in pouch initiation defects similar to *wnt11r* mutants and Alcama localization defects similar to *wnt4a* mutants, as well as suppressing the effects of both Wnt4a and Wnt11r misexpression on epithelial morphology. In the future, investigations aimed at identifying additional co-receptors and/or co-factors should help clarify how Wnt11r and Wnt4a act at least in part through a common Fzd8a receptor to control two distinct phases of pouch epithelial transitions.

Rac and Cdc42 function oppositely in pouch epithelial transitions

One way in which Wnt11r and Wnt4a appear to differentially control pouch epithelial transitions is by activating distinct small GTPases. In particular, our PE-specific transgenic analysis revealed opposite roles for Rac and Cdc42 in the initial destabilization and subsequent remodeling, respectively, of endodermal epithelia into pouch bilayers. Defects in the initial transition of PE cells to a multilayered migratory population upon inhibition of Dvl or Rac function, combined with the increased migratory behavior seen upon constitutive activation of Rac, suggest roles of Dvl and Rac in destabilizing pre-pouch endoderm to allow remodeling and lateral migration. Conversely, the increased membrane accumulation of Alcama and hyper-elongated cell shape seen upon constitutive activation of Cdc42 is consistent with Cdc42 having a preferential role in the Alcama-dependent rearrangements of maturing pouches into bilayers. This function of Cdc42 in pouch cell morphology and rearrangements is also in line with its ability to control cell shape and polarity during *Xenopus* gastrulation (Choi and Han, 2002), pancreatic tubulogenesis (Kesavan et al., 2009), and *Drosophila* embryogenesis (Genova et al., 2000), as well as in yeast (Kelly and Nurse, 2011). Whereas small GTPases are known to act downstream of a number of pathways, several lines of evidence suggest that they act downstream of Wnt signaling during pouch formation. First, loss of Wnt4a, depletion of Fzd8a, and Cdc42 inhibition result in similar mislocalization of Alcama. Second, CA-Cdc42 misexpression restores Alcama localization and elongated pouch cell morphology to embryos lacking Wnt4a or Fzd8a. Third, Cdc42 inhibition suppresses the ability of Wnt4a to induce junctional Alcama enrichment in inappropriate domains of PE. Fourth, Wnt11r and CA-Rac1 misexpression result in similar fragmentation of PE into rosette-like structures. Fifth, CA-Rac1 appears to rescue the migratory behavior of pouch cells in embryos lacking Wnt11r or Fzd8a. Whereas epistasis data support Rac and Cdc42 acting downstream of Wnt11r and Wnt4a, respectively, we cannot rule out that other pathways, such as Fgf signaling (Crump et al., 2004), also impinge on Dvl, Rac, and Cdc42 activity during pouch formation.

Regulatory role of Alcama in epithelial rearrangements and AJ stability

Dynamic regulation of adhesive contacts between cells is essential for epithelial remodeling during development (Villasenor et al., 2010). Cadherins have well-established roles in regulating adhesion and cell sorting (Harris and Tepass, 2008), yet less is known about the role of Ig superfamily members, such as Alcama, in tissue morphogenesis. Strikingly, we find that Alcama has a specific requirement downstream of Wnt4a and Cdc42 for the transition of a multilayered nascent pouch into a bilayered mature pouch. During pouch initiation, we find α-catenin-containing AJs to transiently become more dynamic, suggesting that AJ destabilization helps promote the remodeling and lateral collective migration of pouch-forming cells. As pouches mature, *alcama* becomes expressed through an unknown mechanism, with Cdc42 signaling then targeting Alcama protein to cell-cell contacts. How Cdc42 controls junctional Alcama remains unclear, but Cdc42 has been implicated in the polarized trafficking of other junctional proteins through effects on endocytosis and endosomal recycling (Harris and Tepass, 2008). Significantly, we find that polarized Alcama localization correlates precisely with and is required for the stabilization of α-catenin-containing AJs in maturing pouches. Interestingly, previous reports suggest that junctional localization of Alcama itself may depend on α-catenin, suggesting positive reinforcements between Alcama and AJs (Tomita et al., 2000). An important question then is how Alcama stabilizes AJs. Alcama could associate with components of AJs either directly or through adaptor proteins, yet previous studies have failed to identify binding partners of the short Alcama intracellular domain (Swart et al., 2005). Alternatively, Alcama-mediated homophilic adhesion could indirectly stabilize AJs through physical forces, such as bringing adjacent cell membranes closer together or inhibiting lateral diffusion of AJ complexes. In the future, it will be interesting to examine whether Alcama has similar regulatory adhesion roles in other tissues in which it is expressed, as well as whether Ig-CAMs have more general roles in the restabilization of AJs during epithelial maturation.

EXPERIMENTAL PROCEDURES

Zebrafish lines

wnt4a^{fh295} was identified by TILLING and *wnt11r*^{fh224} has been described (Banerjee et al., 2011). The *wnt4a*^{fh295} mutation changes nucleotide *C*AG to *T*AG and creates a premature stop codon that deletes the C-terminus of the Wnt4a protein, including two highly conserved cysteines critical for the folding of Wnt proteins (Miller, 2002). For genotyping, primers GT150 (5'-GTCAAGACCTGCTGGAAAGC-3') and GT151 (5'-CTTGCGACACTGTTTGCATT-3') were designed to turn *wnt4a*^{fh295} into a co-dominant polymorphism, with a wild-type product of 384 bp and mutant products of 270 and 114 bp after DdeI digestion. Transgenic constructs were generated using the Gateway (Invitrogen) Tol2kit (Kwan et al., 2007); see Extended Experimental Procedures for details. Plasmid DNA was injected with Tol2 transposase RNA (35 ng/μl) into one-cell stage embryos, and stable transgenic lines were isolated for each construct based on transgenic markers – *cmlc2*:GFP for Gal4VP16 lines and *α-crystallin*::Cerulean for UAS lines. 5.9 kb and 5.5 kb of *nkx2.5* and *nkx2.3* upstream regulatory sequence were used to generate *nkx2.5*:Gal4VP16 and *nkx2.3*:Gal4VP16 constructs. For each UAS construct, two to seven independent transgenic lines were crossed to *Tg(nkx2.3:Gal4VP16)*^{el93} and analyzed for phenotypic consistency.

Morpholinos

fzd8a-MO (Kim et al., 2002), *alcama*-MO (Diekmann and Stuermer, 2009), a second independent translation-blocking *fzd8a*-MO-II (5'-ATCCCCAACAGGTAGCACTCCATCC-3'), and an exon2-intron2 splice-blocking *wnt4a*-

MO (5'-CTGTTTCTAATTCTACTAACCTTGT-3') were obtained from Genetools (Eugene, OR, USA). One- to two-cell stage embryos were injected with 5 nl of each MO, and un-injected embryos served as controls.

Immunohistochemistry, in situ hybridization, and skeletal staining

Immunohistochemistry was carried out as previously described with anti-Alcama (ZN8) (Zebrafish International Resource Center, 1:400) and anti-E-cadherin (BD Biosciences, 1:250) (Crump et al., 2004). Whole-mount and fluorescent in situ hybridizations, Alcian blue staining, and GFP immunohistochemistry were performed as described (Zuniga et al., 2011). See Extended Experimental Procedures for probe details.

Imaging

Skeletons and in situ hybridization embryos were imaged on a Zeiss Axioimager.Z1 microscope using Axiovision software. Fluorescence images of antibody-stained or in situ hybridization samples were photographed on a Zeiss LSM5 confocal microscope. For time-lapse imaging, embryos were mounted as previously described (Crump et al., 2004) and confocal images were taken every 10 minutes using a Zeiss LSM510Meta confocal microscope. Approximately 100 μm Z-stacks at 3.5 μm intervals were captured with a Zeiss 20X LD-Plan Neofluar objective lens, or 80 μm Z-stacks at 1.5 μm intervals with a Zeiss 40X LD-Plan Neofluar objective lens. Cell tracking and speed measurements were performed using Fiji. Cell centroids were tracked for those cells that could be definitively followed through the entire movie. The profile tool within the ZEN software was used to quantitate Alcama and E-cadherin fluorescence intensity. For normalization, the brightness of non-fluorescent regions was adjusted to zero and then the maximum fluorescence intensity was adjusted to 100 by adjusting the contrast. Care was taken to process all images in an identical manner.

Fluorescence correlation spectroscopy

FCS experiments were done using a 40x 1.2NA C-Apochromat water immersion objective specifically calibrated for a LSM710 microscope and CONFOCOR3 software (Zeiss). A single point in the apical membrane was chosen and the fluorescence fluctuation within the designated confocal volume recorded for 5 seconds. The recording was repeated 5 times. For autocorrelation fitting, the first scan was always discarded as the raw count data slopes downward because of bleaching of non-mobile protein. The remaining scans were looked at individually, discarded if they showed any sloping or sudden discontinuity, and then averaged to generate the final data plot for that point. Remaining fluorescence fluctuation data were then fitted to a mathematical model, generating the autocorrelation curve from which the diffusion coefficient in μm^2/second was derived (Haustein and Schwille, 2007). Data analysis was performed using the FCS module in the ZEN software (Zeiss). A one-component 3D diffusion model was used with the blinking time fixed to 625 μs and the structural parameter fixed to 5. The data fits were done starting at 200 μs. The diffusion time (t) was calculated from the autocorrelation curve and used to determine the diffusion coefficient (D) using the equation $t = wr^2/(4D)$. The beam radius (wr) was 0.22.

Statistics

We employed the Fisher's Exact Test for rescue of *alcama*-MO defects and quantifying *wnt4a*- defects, and a one-tailed student's t-test with unequal variance for quantifying cell shape changes, diffusion coefficients of α-catenin, pouch cell speed, and pouch defects in mutant, MO, and transgenic embryos.

Supplementary Material

Refer to Web version on PubMed Central for supplementary material.

Acknowledgments

We thank Debbie Yelon and Henry Sucov for comments. C.P.C. was funded by a CIRM training grant. A.C. was supported by the Kleberg and Ahmanson Foundations. The identification of the *wnt4a* mutant was funded by an NIH HG002995 grant to C.B.M. C.B.M. is an investigator with the Howard Hughes Medical Institute. *Gt(ctnna-citrine)*^{ct3a} was identified in a FlipTrap screen funded by a NHGRI Center for Excellence in Genomic Science P50HG004071 grant to L.A.T.

References

Abo A, Pick E, Hall A, Totty N, Teahan CG, Segal AW. Activation of the NADPH oxidase involves the small GTP-binding protein p21rac1. Nature. 1991; 353:668–670. [PubMed: 1922386]

Axelrod JD, Miller JR, Shulman JM, Moon RT, Perrimon N. Differential recruitment of Dishevelled provides signaling specificity in the planar cell polarity and Wingless signaling pathways. Genes Dev. 1998; 12:2610–2622. [PubMed: 9716412]

Banerjee S, Gordon L, Donn TM, Berti C, Moens CB, Burden SJ, Granato M. A novel role for MuSK and non-canonical Wnt signaling during segmental neural crest cell migration. Development. 2011; 138:3287–3296. [PubMed: 21750038]

Choi SC, Han JK. Xenopus Cdc42 regulates convergent extension movements during gastrulation through Wnt/Ca2+ signaling pathway. Dev Biol. 2002; 244:342–357. [PubMed: 11944942]

Choudhry P, Joshi D, Funke B, Trede N. Alcama mediates Edn1 signaling during zebrafish cartilage morphogenesis. Developmental biology. 2011; 349:483–493. [PubMed: 21073867]

Couly G, Le Douarin NM. Head morphogenesis in embryonic avian chimeras: evidence for a segmental pattern in the ectoderm corresponding to the neuromeres. Development. 1990; 108:543–558. [PubMed: 2387234]

Crump JG, Maves L, Lawson ND, Weinstein BM, Kimmel CB. An essential role for Fgfs in endodermal pouch formation influences later craniofacial skeletal patterning. Development. 2004; 131:5703–5716. [PubMed: 15509770]

Curado S, Stainier DY, Anderson RM. Nitroreductase-mediated cell/tissue ablation in zebrafish: a spatially and temporally controlled ablation method with applications in developmental and regeneration studies. Nat Protoc. 2008; 3:948–954. [PubMed: 18536643]

Dequeant ML, Pourquie O. Segmental patterning of the vertebrate embryonic axis. Nat Rev Genet. 2008; 9:370–382. [PubMed: 18414404]

Diekmann H, Stuermer CA. Zebrafish neurolin-a and -b, orthologs of ALCAM, are involved in retinal ganglion cell differentiation and retinal axon pathfinding. J Comp Neurol. 2009; 513:38–50. [PubMed: 19107846]

Eaton S, Auvinen P, Luo L, Jan YN, Simons K. CDC42 and Rac1 control different actin-dependent processes in the Drosophila wing disc epithelium. The Journal of cell biology. 1995; 131:151–164. [PubMed: 7559772]

Feig LA. Tools of the trade: use of dominant-inhibitory mutants of Ras-family GTPases. Nature cell biology. 1999; 1:E25–27.

Friedl P, Gilmour D. Collective cell migration in morphogenesis, regeneration and cancer. Nature reviews Molecular cell biology. 2009; 10:445–457.

Genova JL, Jong S, Camp JT, Fehon RG. Functional analysis of Cdc42 in actin filament assembly, epithelial morphogenesis, and cell signaling during Drosophila development. Developmental biology. 2000; 221:181–194. [PubMed: 10772800]

Gessert S, Maurus D, Brade T, Walther P, Pandur P, Kuhl M. DM-GRASP/ALCAM/CD166 is required for cardiac morphogenesis and maintenance of cardiac identity in first heart field derived cells. Dev Biol. 2008; 321:150–161. [PubMed: 18598690]

Graham A. The development and evolution of the pharyngeal arches. J Anat. 2001; 199:133–141. [PubMed: 11523815]

Graham A. Deconstructing the pharyngeal metamere. J Exp Zool B Mol Dev Evol. 2008; 310:336–344. [PubMed: 17583579]

Graham A, Okabe M, Quinlan R. The role of the endoderm in the development and evolution of the pharyngeal arches. J Anat. 2005; 207:479–487. [PubMed: 16313389]

Harris KP, Tepass U. Cdc42 and Par proteins stabilize dynamic adherens junctions in the Drosophila neuroectoderm through regulation of apical endocytosis. The Journal of cell biology. 2008; 183:1129–1143. [PubMed: 19064670]

Haustein E, Schwille P. Fluorescence correlation spectroscopy: novel variations of an established technique. Annu Rev Biophys Biomol Struct. 2007; 36:151–169. [PubMed: 17477838]

Hogan BL, Kolodziej PA. Organogenesis: molecular mechanisms of tubulogenesis. Nat Rev Genet. 2002; 3:513–523. [PubMed: 12094229]

Hutterer A, Betschinger J, Petronczki M, Knoblich JA. Sequential roles of Cdc42, Par-6, aPKC, and Lgl in the establishment of epithelial polarity during Drosophila embryogenesis. Developmental cell. 2004; 6:845–854. [PubMed: 15177032]

Jacobson AG. Somitomeres: mesodermal segments of vertebrate embryos. Development. 1988; 104(Suppl):209–220. [PubMed: 3077109]

Kelly FD, Nurse P. Spatial control of Cdc42 activation determines cell width in fission yeast. Mol Biol Cell. 2011; 22:3801–3811. [PubMed: 21849474]

Kesavan G, Sand FW, Greiner TU, Johansson JK, Kobberup S, Wu X, Brakebusch C, Semb H. Cdc42-mediated tubulogenesis controls cell specification. Cell. 2009; 139:791–801. [PubMed: 19914171]

Kim SH, Shin J, Park HC, Yeo SY, Hong SK, Han S, Rhee M, Kim CH, Chitnis AB, Huh TL. Specification of an anterior neuroectoderm patterning by Frizzled8a-mediated Wnt8b signalling during late gastrulation in zebrafish. Development. 2002; 129:4443–4455. [PubMed: 12223403]

Kusserow A, Pang K, Sturm C, Hrouda M, Lentfer J, Schmidt HA, Technau U, von Haeseler A, Hobmayer B, Martindale MQ, et al. Unexpected complexity of the Wnt gene family in a sea anemone. Nature. 2005; 433:156–160. [PubMed: 15650739]

Kwan KM, Fujimoto E, Grabher C, Mangum BD, Hardy ME, Campbell DS, Parant JM, Yost HJ, Kanki JP, Chien CB. The Tol2kit: a multisite gateway-based construction kit for Tol2 transposon transgenesis constructs. Dev Dyn. 2007; 236:3088–3099. [PubMed: 17937395]

Lawrence PA, Casal J, Struhl G. Towards a model of the organisation of planar polarity and pattern in the Drosophila abdomen. Development. 2002; 129:2749–2760. [PubMed: 12015301]

Lee KH, Xu Q, Breitbart RE. A new tinman-related gene, nkx2.7, anticipates the expression of nkx2.5 and nkx2.3 in zebrafish heart and pharyngeal endoderm. Developmental biology. 1996; 180:722–731. [PubMed: 8954740]

Matsui T, Raya A, Kawakami Y, Callol-Massot C, Capdevila J, Rodriguez-Esteban C, Izpisua Belmonte JC. Noncanonical Wnt signaling regulates midline convergence of organ primordia during zebrafish development. Genes Dev. 2005; 19:164–175. [PubMed: 15630025]

Meier S. Development of the chick embryo mesoblast. Formation of the embryonic axis and establishment of the metameric pattern. Dev Biol. 1979; 73:24–45. [PubMed: 527768]

Miller JR. The Wnts. Genome Biol. 2002; 3 REVIEWS3001.

Molenaar M, van de Wetering M, Oosterwegel M, Peterson-Maduro J, Godsave S, Korinek V, Roose J, Destree O, Clevers H. XTcf-3 transcription factor mediates beta-catenin-induced axis formation in Xenopus embryos. Cell. 1996; 86:391–399. [PubMed: 8756721]

Nishimura T, Takeichi M. Remodeling of the adherens junctions during morphogenesis. Curr Top Dev Biol. 2009; 89:33–54. [PubMed: 19737641]

O'Rahilly R. The timing and sequence of events in the development of the human digestive system and associated structures during the embryonic period proper. Anat Embryol (Berl). 1978; 153:123–136. [PubMed: 677467]

Ober EA, Verkade H, Field HA, Stainier DY. Mesodermal Wnt2b signalling positively regulates liver specification. Nature. 2006; 442:688–691. [PubMed: 16799568]

Park TJ, Mitchell BJ, Abitua PB, Kintner C, Wallingford JB. Dishevelled controls apical docking and planar polarization of basal bodies in ciliated epithelial cells. Nat Genet. 2008; 40:871–879. [PubMed: 18552847]

Peters H, Neubuser A, Kratochwil K, Balling R. Pax9-deficient mice lack pharyngeal pouch derivatives and teeth and exhibit craniofacial and limb abnormalities. Genes Dev. 1998; 12:2735–2747. [PubMed: 9732271]

Piotrowski T, Nusslein-Volhard C. The endoderm plays an important role in patterning the segmented pharyngeal region in zebrafish (Danio rerio). Dev Biol. 2000; 225:339–356. [PubMed: 10985854]

Ries J, Yu SR, Burkhardt M, Brand M, Schwille P. Modular scanning FCS quantifies receptor-ligand interactions in living multicellular organisms. Nat Methods. 2009; 6:643–645. [PubMed: 19648917]

Schlessinger K, Hall A, Tolwinski N. Wnt signaling pathways meet Rho GTPases. Genes Dev. 2009; 23:265–277. [PubMed: 19204114]

Sisson BE, Topczewski J. Expression of five frizzleds during zebrafish craniofacial development. Gene Expr Patterns. 2009; 9:520–527. [PubMed: 19595791]

Swart GW, Lunter PC, Kilsdonk JW, Kempen LC. Activated leukocyte cell adhesion molecule (ALCAM/CD166): signaling at the divide of melanoma cell clustering and cell migration? Cancer Metastasis Rev. 2005; 24:223–236. [PubMed: 15986133]

Tallafuss A, Bally-Cuif L. Tracing of her5 progeny in zebrafish transgenics reveals the dynamics of midbrain-hindbrain neurogenesis and maintenance. Development. 2003; 130:4307–4323. [PubMed: 12900448]

Tomita K, van Bokhoven A, Jansen CF, Bussemakers MJ, Schalken JA. Coordinate recruitment of E-cadherin and ALCAM to cell-cell contacts by alpha-catenin. Biochem Biophys Res Commun. 2000; 267:870–874. [PubMed: 10673383]

van de Wetering M, Sancho E, Verweij C, de Lau W, Oving I, Hurlstone A, van der Horn K, Batlle E, Coudreuse D, Haramis AP, et al. The beta-catenin/TCF-4 complex imposes a crypt progenitor phenotype on colorectal cancer cells. Cell. 2002; 111:241–250. [PubMed: 12408868]

Villasenor A, Chong DC, Henkemeyer M, Cleaver O. Epithelial dynamics of pancreatic branching morphogenesis. Development. 2010; 137:4295–4305. [PubMed: 21098570]

Wang YC, Khan Z, Kaschube M, Wieschaus EF. Differential positioning of adherens junctions is associated with initiation of epithelial folding. Nature. 2012; 484:390–393. [PubMed: 22456706]

Witzel HR, Jungblut B, Choe CP, Crump JG, Braun T, Dobreva G. The LIM Protein Ajuba Restricts the Second Heart Field Progenitor Pool by Regulating Isl1 Activity. Developmental cell. 2012; 23:58–70. [PubMed: 22771034]

Wodarz A, Nusse R. Mechanisms of Wnt signaling in development. Annu Rev Cell Dev Biol. 1998; 14:59–88. [PubMed: 9891778]

Yoo SK, Deng Q, Cavnar PJ, Wu YI, Hahn KM, Huttenlocher A. Differential regulation of protrusion and polarity by PI3K during neutrophil motility in live zebrafish. Dev Cell. 2010; 18:226–236. [PubMed: 20159593]

Zuniga E, Rippen M, Alexander C, Schilling TF, Crump JG. Gremlin 2 regulates distinct roles of BMP and Endothelin 1 signaling in dorsoventral patterning of the facial skeleton. Development. 2011; 138:5147–5156. [PubMed: 22031546]

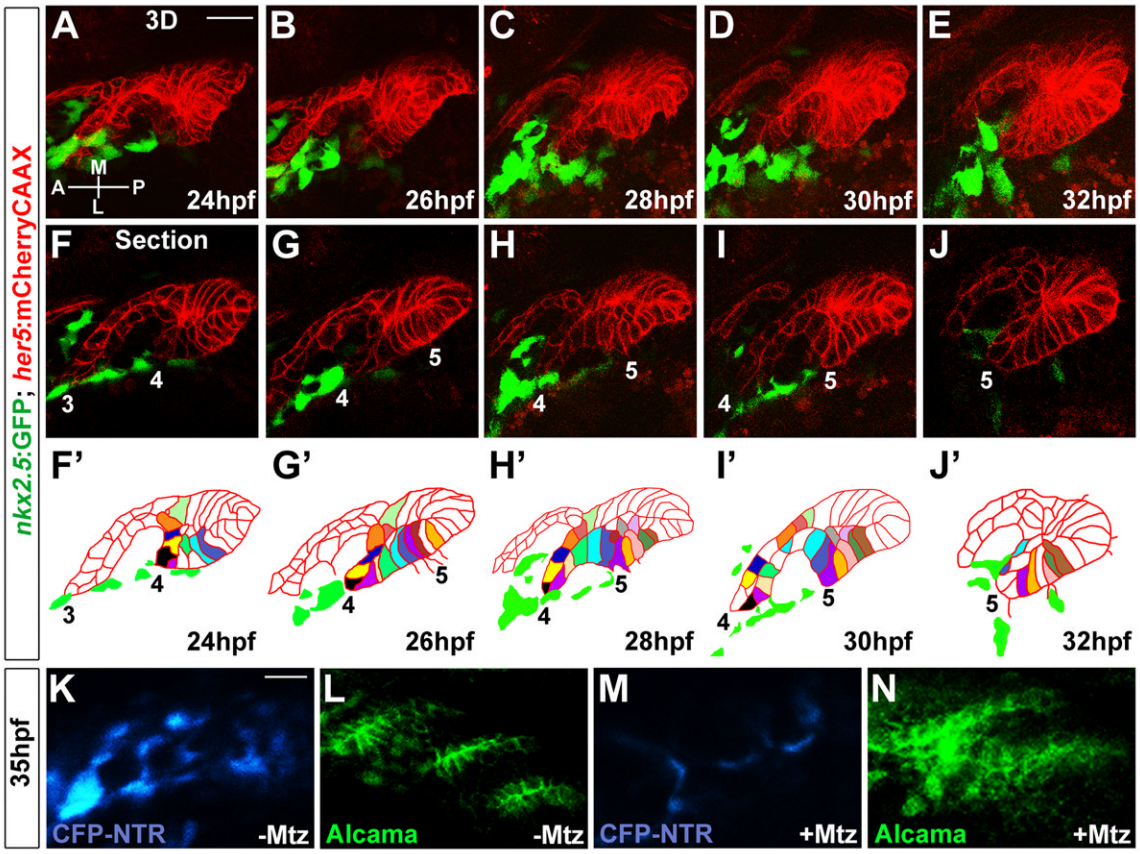

Figure 1. *nkx2.5*-expressing mesoderm guides pouch epithelial transitions

(A-E) 3D projections captured from time-lapse recording of wild-type pouch development (See Movie S2) show intimate interactions between *her5*:mCherryCAAX-positive endodermal epithelia (red) and *nkx2.5*:GFP-positive mesoderm (green). Anterior-posterior (A-P) and medial-lateral (M-L) axes are shown.

(F-J) Representative sections from the same time-lapse recording (see Movie S2) show various stages of development of pouches 3-5. In the schematics (F'-J'), the tracking of individually color-coded pouch cells highlights cell rearrangements. Cells that we could not track through the entire recording were left uncolored.

(K-N) CFP fluorescence (blue) and Alcama immunohistochemistry (green) show that injection of 5 nl of 5 mM Mtz into *nkx2.5*:Gal4VP16; UAS:CFP-NTR embryos results in reductions of CFP-NTR-expressing mesoderm and disorganized pouch endoderm (M and N) compared to un-injected siblings (K and L). Scale bars = 20 μM.

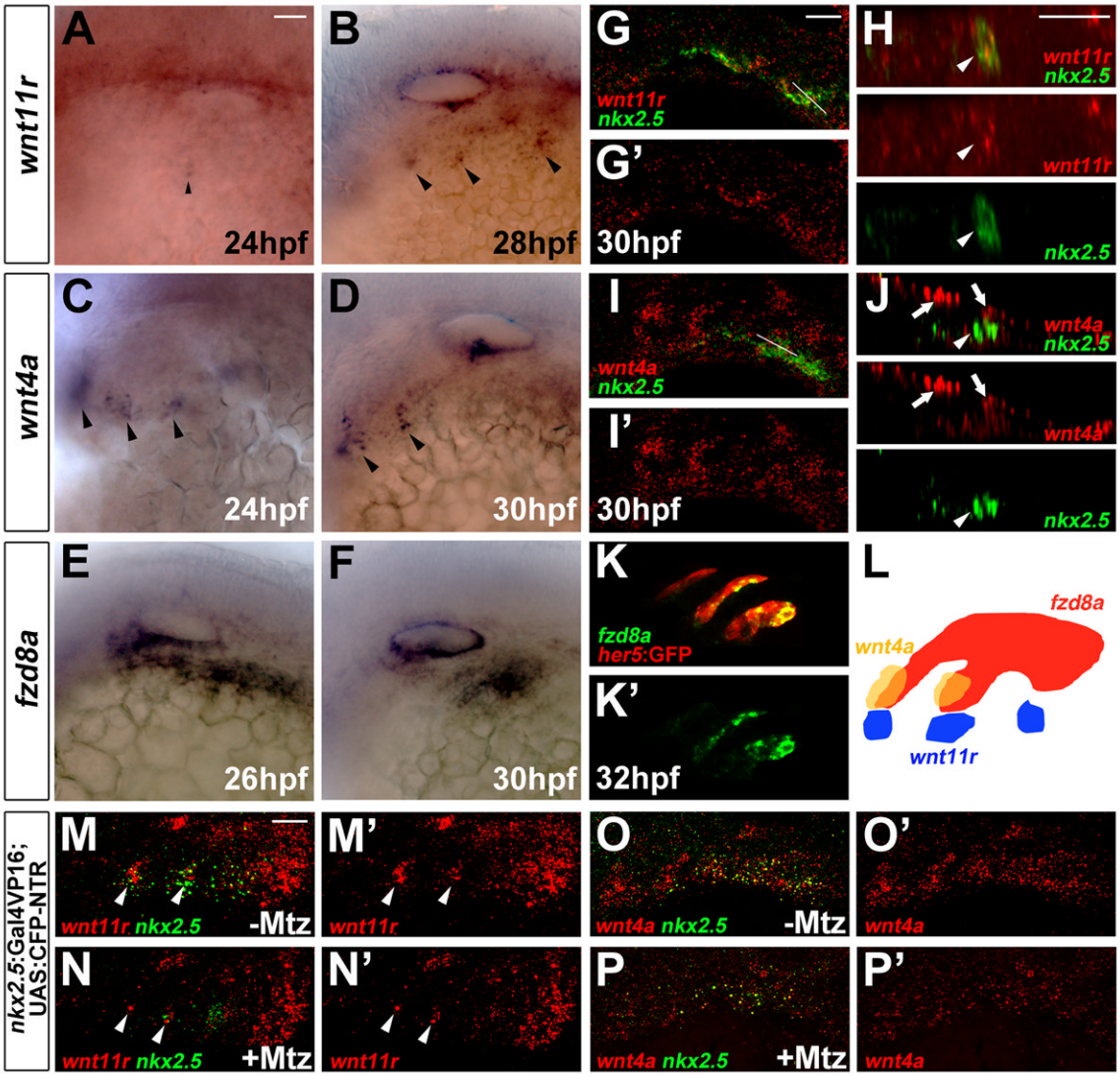

Figure 2. Expression of *wnt11r*, *wnt4a*, and *fzd8a* during pouch formation

(A-F) Colorimetric in situs show expression of *wnt11r* in discrete domains of mesoderm (arrowheads in A and B), *wnt4a* in ectodermal patches (arrowheads in C and D), and *fzd8a* in pouch-forming endoderm (E and F).

(G-J) Double fluorescent in situs show co-localization of *wnt11r* but not *wnt4a* with *nkx2.5* in lateral views (G and I) and higher magnification orthogonal sections (H and J, taken at level of white lines in G and I). Arrowheads indicate mesoderm and arrows ectoderm.

(K) Fluorescent in situ shows co-localization of *fzd8a* (green) with *her5*-positive pouch endoderm labeled by GFP immunohistochemistry (red).

(L) Schematic showing expression of *wnt11r* in mesoderm (blue), *wnt4a* in ectoderm (yellow), and *fzd8a* in endoderm (red) during pouch formation.

(M-P) Compared to un-injected siblings (M and O), injection of 5 nl of 5 mM Mtz into *nkx2.5*:Gal4VP16; UAS:CFP-NTR embryos results in reduced numbers of mesodermal cells expressing *nkx2.5* and *wnt11r* (arrowheads), as well as reduced ectodermal *wnt4a* expression. Scale bars = 20 μM.

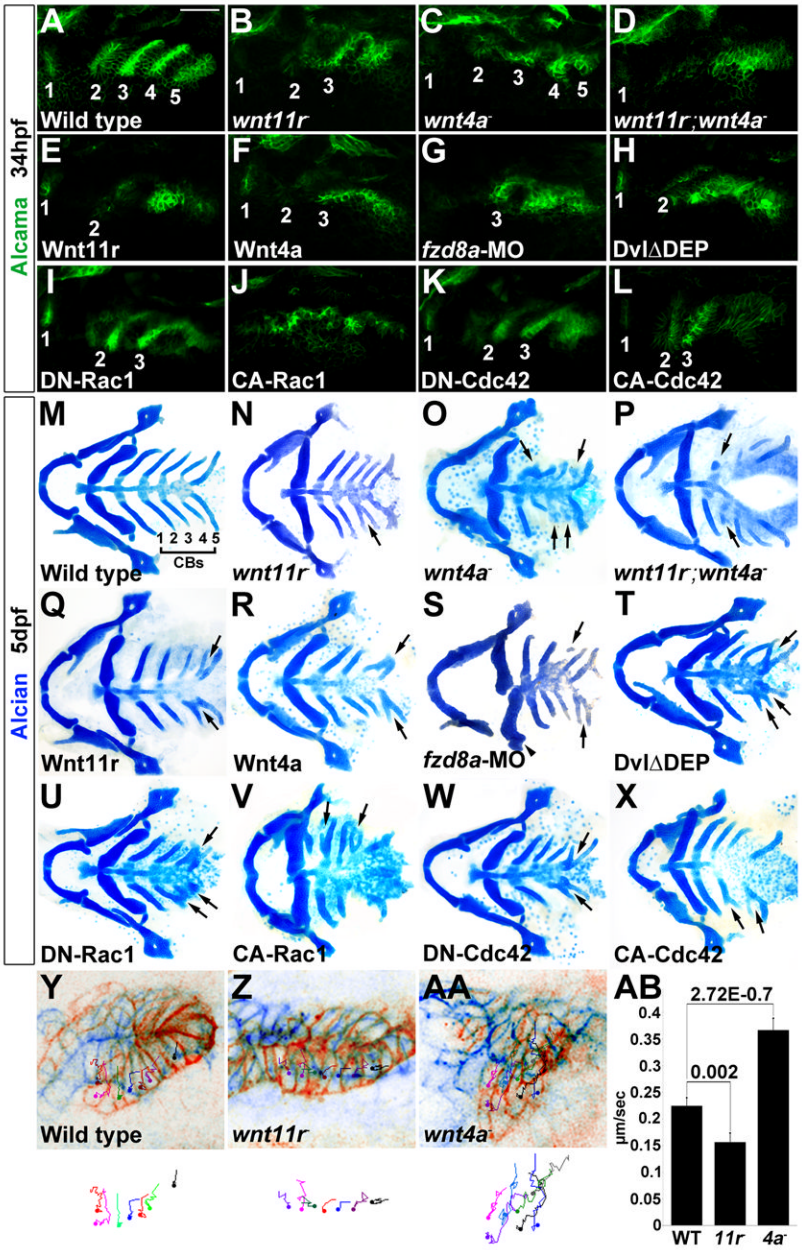

Figure 3. Roles of Wnt signaling components in pouch and CB cartilage development

(A-L) Alcama immunohistochemistry (green) shows defects in pouches in mutant, *fzd8a*-MO, and transgenic embryos. Identifiable pouches are numbered. UAS transgenic embryos (capitalized) were doubly positive for *nkx2.3*:Gal4VP16. Scale bar = 40 μM.

(M-X) Whole mount views of dissected facial cartilages. Arrows indicated fused or abnormal CB cartilages. Arrowhead indicates abnormal hyoid cartilage in *fzd8a*-MO embryos.

(Y-AA) Superimposition of initial (blue) and final (red) still images from time-lapse recordings of fifth pouch development in wild-type, *wnt11r*$^{-/-}$, and *wnt4a*$^{-/-}$ embryos. Colored lines indicate cell tracks (shown also below merged images), with filled circles denoting final positions.

(AB) Average pouch cell speed in wild types and mutants. Data represent mean ± SEM and *p*-values are shown for each comparison.
See also Figures S1 and S2.

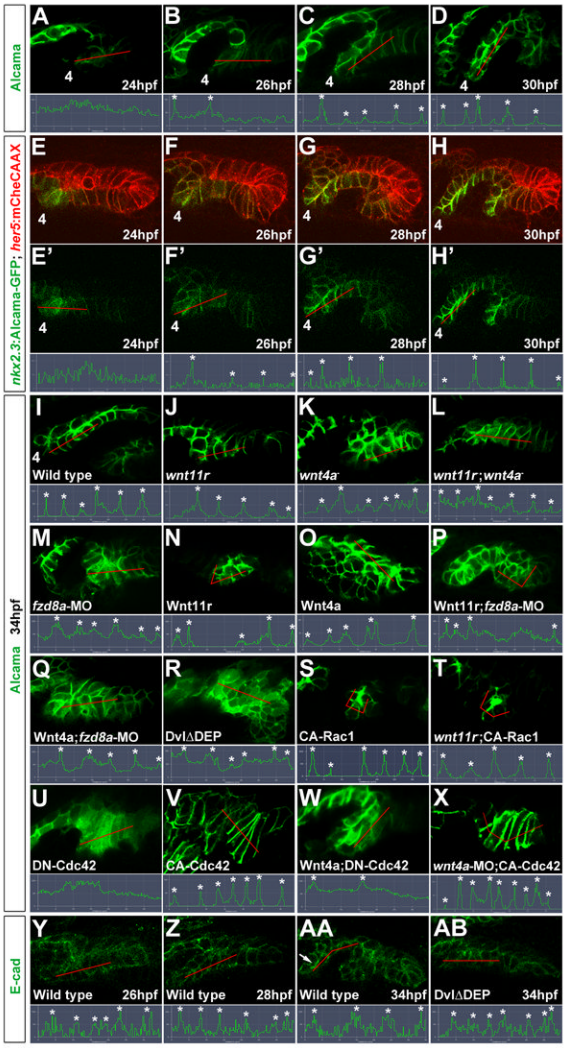

Figure 4. Wnt signaling and Cdc42 regulate junctional localization of Alcama in developing pouches

(A-D) Immunohistochemistry shows progressive junctional localization of Alcama in the wild-type fourth pouch. Below each image, the normalized intensity of fluorescent signal is plotted along the 35 μM red lines. Asterisks indicate clear cell-cell boundaries.

(E-H) Still images from a time-lapse confocal recording of fourth pouch development in *nkx2.3*:Alcama-GFP; *her5*:mCherryCAAX transgenic embryos (see Movie S6). As with endogenous Alcama protein, plots of fluorescence intensity through the red lines show progressive junctional localization of Alcama-GFP (green) within *her5*:mCherryCAAX-positive pouch cells (red).

(I-X) Immunohistochemistry shows Alcama localization at the level of the fourth pouch in wild-type, mutant, and *fzd8a*-MO embryos, as well as UAS transgenic embryos (capitalized) doubly positive for *nkx2.3*:Gal4VP16. Alcama is partially mislocalized from pouch cell membranes to the cytoplasm in *wnt4a*$^{-}$, *wnt11r*$^{-}$;*wnt4a*$^{-}$, and *fzd8a*-MO embryos but not in *wnt11r*$^{-}$ embryos. In contrast, misexpression of Wnt11r results in disorganized endoderm (n=28/32, data not shown) and occasionally rosette-like structures (n=3/32), with rosette-like structures never observed in *fzd8a*-MO-injected siblings (n=0/23, p= 0.003). Similarly, the inappropriate Alcama junctional localization induced by Wnt4a misexpression (n=26/114) was never seen in *fzd8a*-MO-injected siblings (n=0/74, p=0.004) or doubly transgenic

Wnt4a; DN-Cdc42 embryos (n=0/31, p=0.005). Rosette-like structures were observed in both CA-Rac1 embryos (n=104/112) and their *wnt11r* mutant siblings (n=11/17), and hyper-elongated pouches were observed in both CA-Cdc42 embryos (n=85/122) and their *wnt4a*-MO-injected siblings (n=72/101). Plots of fluorescence intensity through the red lines are shown, with asterisks indicating clear cell-cell junctions.

(Y-AB) Immunohistochemistry and normalized line plots show junctional localization of E-cadherin throughout wild-type pouch development, with pronounced apical enrichment (arrow in AA) as pouches mature. Inhibition of Dvl in *nkx2.3*:Gal4VP16; *UAS*:DvlΔDEP embryos does not significantly disrupt E-cadherin localization.

See also Figure S3.

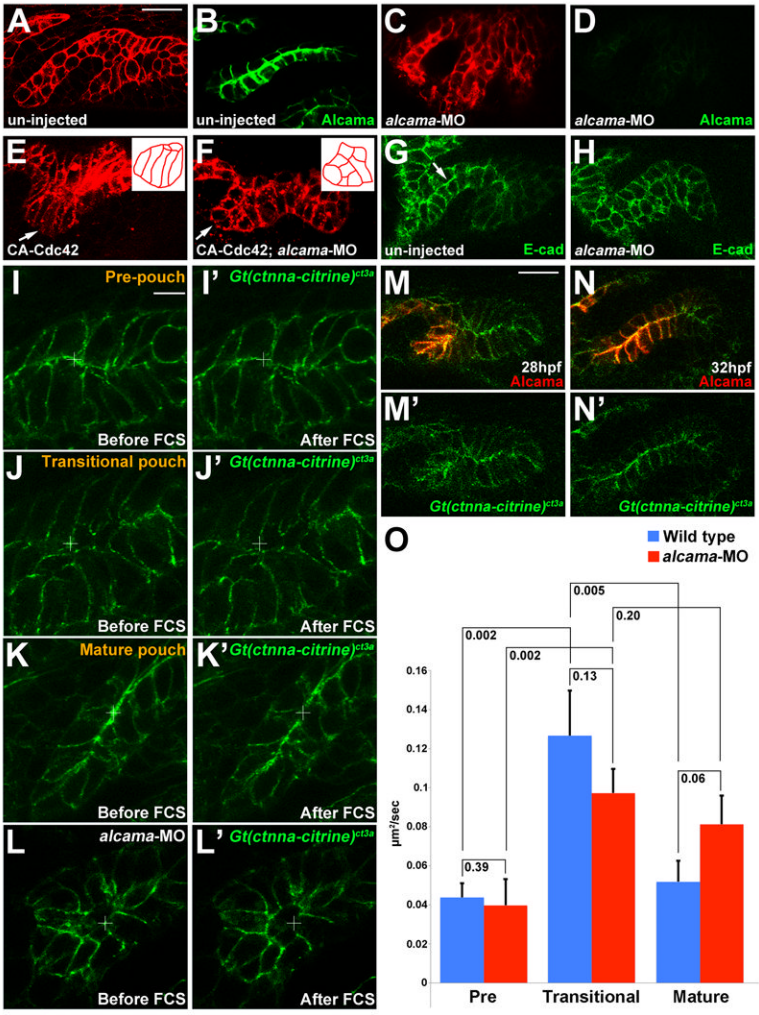

Figure 5. Alcama is required for pouch bilayer formation and AJ stabilization

(A-D) *her5*:mCherryCAAX fluorescence (red) and Alcama immunohistochemistry (green) show loss of Alcama protein and an aberrant multilayered pouch morphology in *alcama*-MO embryos (C and D) compared to un-injected controls (A and B). Scale bar = 20 μM.

(E and F) *her5*:mCherryCAAX labeling shows that the elongated morphology of pouch cells (arrows) resulting from CA-Cdc42 misexpression (n=49/72) is suppressed by Alcama depletion (n=0/67). Insets show schematics of pouch cell morphology.

(G and H) Immunohistochemistry shows that E-cadherin still localizes to cell-cell junctions in the absence of Alcama protein yet the apical enrichment seen in wild-type mature pouches (arrow) is missing.

(I-L) Imaging of α-catenin localization during three phases of wild-type pouch formation (I-K) and during a comparable phase of *alcama*-MO development (L) when wild-type pouches would have matured into bilayers. Crosshairs show target regions before FCS laser illumination (I-L) and 25 seconds after (I'-L'). Scale bar = 5 μM.

(M and N) Alcama immunohistochemistry in wild-type *Gt(ctnna-citrine)*^{ct3a} embryos shows that the appearance of Alcama (red) at apical and lateral cell-cell junctions corresponds to a transition from disorganized to strongly apical localization of α-catenin (green). Scale bar = 20 μM.

(O) FCS measurements of endogenous α-catenin mobility in wild-type embryos show a significant increase in mobility from pre-pouch to transitional endoderm and a subsequent

decrease in mature bilayers. In *alcama*-MO embryos, α-catenin mobility increases from pre-pouch to transitional endoderm but fails to decrease at a stage comparable to the mature wild-type pouch. n=16 for each. Data represent mean ± SEM and *p*-values are shown for each comparison.
See also Figure S4.

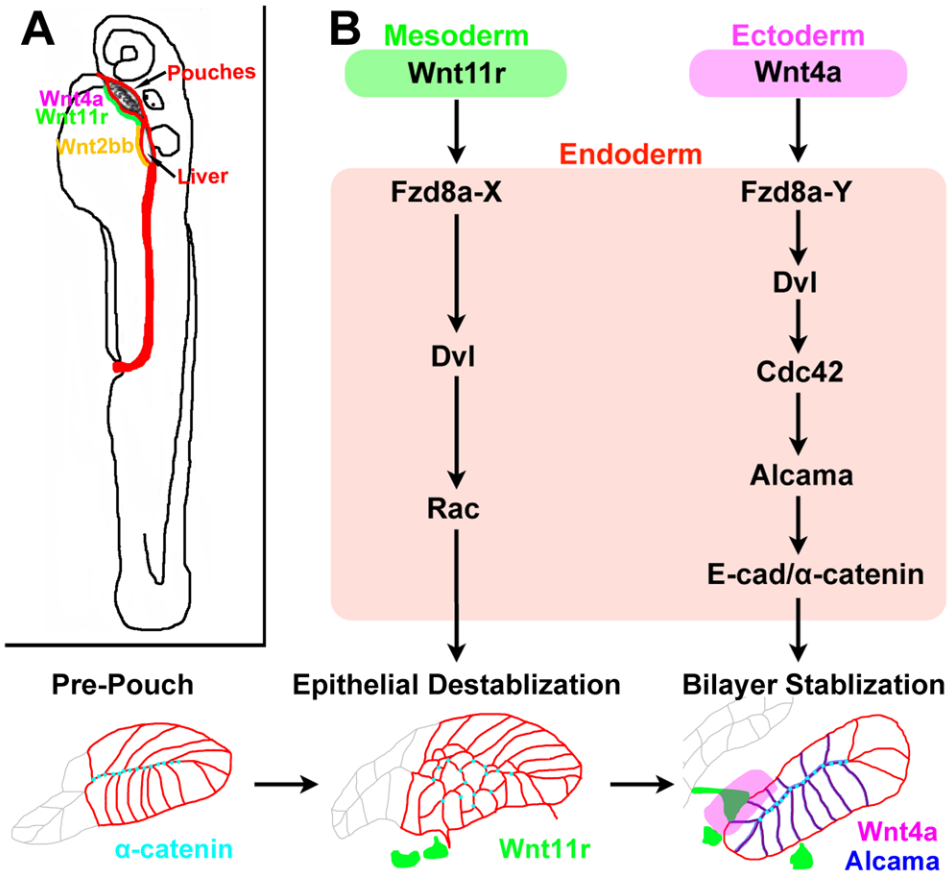

Figure 6. Model of pouch formation

(A) Wnt4a and Wnt11r may play analogous roles to Wnt2bb during the budding of the endodermal pouches and liver, respectively. The embryonic endoderm is shown in red and mesodermal Wnt11r and Wnt2bb in green and yellow, respectively.

(B) Distinct genetic pathways downstream of mesodermal Wnt11r and ectodermal Wnt4a mediate the initial destabilization and subsequent remodeling of the Fzd8a-expressing endodermal epithelium. We hypothesize that distinct types of co-receptors or co-factors (X and Y) could mediate different outputs of Wnt11r-Fzd8a and Wnt4a-Fzd8a activation.

Table 1

Summary of pouch, CB cartilage, and Alcama localization defects.

Genotype	$n^{Pouches}$	Pouches	Loss of ≥2 Pouches	Loss of 1 Pouch	Abnormal, No Loss	Normal	*p*-value	n^{CBs}	CBs	n^{Alcama}	Alcama Localization
Wild type	100	5.0	0%	0%	0%	100%		100	5.0	55	0.07
wnt11r^{-}	222	4.3 (4-5)	0%	46%	19%	35%	6.61E-40[a]	131	4.6 (4-5)	58	0.17
wnt4a^{-}	352	5.0 (5)	0%	0%	23%	77%	5.71E-08[b]	144	4.1 (3-5)	51	0.53
wnt11r^{-}*; wnt4a*$^{-}$	45	3.4 (2-4)	20%	47%	0%	33%	5.97E-12[a]	16	3.7 (2-4)	59	0.69
wnt4a-MO	98	4.6 (4-5)	0%	20%	26%	54%	2.12E-07[a]	74	3.8 (3-5)	61	0.52
wnt11r^{-}*; wnt4a*-MO	56	3.0 (2-4)	50%	25%	0%	25%	2.82E-13[c]	48	3.4 (1-5)	51	0.71
fzd8a-MO (200uM)	260	3.9 (2-5)	18%	26%	24%	32%	1.42E-29[a]	253	3.8 (2-5)	58	0.69
fzd8a-MO (100uM)	86	5.0 (5)	0%	0%	0%	100%		78	5.0	n/a	n/a
fzd8a-MO-II	212	3.9 (2-5)	19%	32%	19%	30%	1.87E-32[a]	87	3.9 (2-5)	53	0.66
wnt11r^{-}*; fzd8a*-MO (200uM)	62	3.9 (2-5)	19%	35%	23%	23%	0.4977[d]	68	3.9 (2-5)	64	0.73
wnt11r^{-}*; fzd8a*-MO (100uM)	44	4.0 (2-5)	7%	55%	7%	31%	0.0238[c]	38	4.1 (3-5)	55	0.64
wnt4a^{-}*; fzd8a*-MO (200uM)	61	4.0 (2-5)	18%	35%	21%	26%	0.3328[d]	65	3.8 (2-5)	64	0.78
wnt4a^{-}*; fzd8a*-MO (100uM)	42	4.0 (3-5)	17%	29%	14%	40%	1.29E-07[e]	40	4.0 (2-5)	51	0.67
wnt11r^{-}*; wnt4a*$^{-}$; *fzd8a*-MO (200uM)	36	2.9 (2-4)	86%	6%	0%	8%	0.0185[f]	28	3.3 (2-5)	57	0.86
nkx2.3:Gal4VP16^{el93}	78	5.0	0%	0%	0%	100%		75	5.0	52	0.09
UAS:Wnt11r^{el421}	32	3.2 (2-4)	50%	38%	0%	12%	3.19E-13[g]	33	3.5 (3-4)	51	0.24
UAS:Wnt4a^{el48}	114	3.4 (3-4)	42%	39%	0%	19%	1.05E-24[g]	70	3.7 (3-4)	66	0.06
UAS:DvlΔDEP^{el190}	122	2.8 (2-4)	74%	15%	0%	11%	9.72E-30[g]	68	3.4 (2-4)	62	0.84
UAS:DN-Rac1^{el262}	152	3.4 (3-4)	41%	27%	0%	32%	4.34E-29[g]	77	3.8 (3-4)	68	0.63
UAS:DN-Cdc42^{el268}	124	3.9 (3-5)	11%	58%	10%	21%	1.50E-18[g]	82	3.6 (2-4)	65	0.85

Dev Cell. Author manuscript; available in PMC 2013 August 11.

Genotype	$n^{Pouches}$	Pouches	Loss of ≥2 Pouches	Loss of 1 Pouch	Abnormal, No Loss	Normal	*p*-value	n^{CBs}	CBs	n^{Alcama}	Alcama Localization
UAS:CA-Rac1^{el320}	112	1.4 (0-3)	93%	0%	0%	7%	2.25E-30[g]	58	1.8 (1-3)	55	0.18
UAS:CA-Cdc42^{el322}	138	3.1 (2-4)	44%	27%	0%	29%	7.43E-22[g]	64	3.2 (3-4)	50	0.02

UAS transgenes were doubly transgenic with *nkx2.3*:Gal4VP16. The number (*n*) of analyzed embryos of each genotype is indicated for pouches and CB cartilages, with *n* for Alcama localization representing total number of cells analyzed. For pouches and CBs, the average number of identifiable separate elements is listed with the range of numbers in parentheses. For the scoring of Alcama localization (expressed as an average), strong membrane signal with either no or weak cytoplasmic signal was counted as 0, whereas strong cytoplasmic signal was counted as 1. *p*-values for differences in pouch number were calculated for the following comparisons:

[a] wild type,

[c] *wnt11r*,

[d] *fzd8a*-MO (200uM),

[e] *wnt4a*,

[f] *wnt11r;wnt4a*,

[g] and *nkx2.3*:Gal4VP16,

[b] and for the difference in pouch morphology versus wild type.